Hydrodynamic assessment of a dual-rotor horizontal axis marine current turbine

Abstract

The hydrodynamic performance of a dual-rotor horizontal axis marine turbine (HAMCT) is investigated for the power gain in operating the rear rotor without blade-pitch control. This kind of turbine can be advantageous for a rectilinear tidal current of reversing directions, where each rotor blade is optimally fixed-pitched towards its upstream velocity. The blade element momentum (BEM) method is coupled with the Park wake model. A generic three-blade turbine is shown to gain up to 20% in the coefficient of power C_P as relative to the front rotor C_P when operating the rear rotor at the same tip speed ratio (TSR) as the front one, gaining overall C_P up to 0.55. Analytic model is derived to backup the estimate of power gain. Plots for turbine performance variation with TSR and profile hydrodynamic efficiency are given, and analysed for lab and small-medium size turbines.

Keywords: Rectilinear tidal current, horizontal-axis turbine, dual-rotor, hydrodynamics

1. Introduction

Marine energy has an abundant potential around the world, where the tidal energy industry is emerging as a promising sector. Tidal energy has two main forms that can be harnessed; tidal wave energy and tidal current energy. The focus of this study is on hydro-kinetic turbines that extract power from tidal currents. In the early days, such energy was extracted by building barrages along the coast, which required a significant financial investment and could have a considerable effect on the environment (Charlier, 2003). Recent developments in hydro-kinetic turbines and the identification of sites around the world with high tidal energy as the Edy island in the UK and the Gulf of Kutal in India, mean that the build up of such barrages is not a necessary condition any more (Charlier, 2003).

Hydro-kinetic turbines can come in several forms but there are two basic configurations of a horizontal axis or a vertical axis turbine. The vertical axis turbine can be lift or drag based device. The drag-based device is typically limited to low speed ratio (TSR) and the lift-based device excels at high TSR, where $TSR=\Omega R/V$, Ω is the rotational speed of the turbine, e.g. round per minute (RPM), R is its radius and V is the incoming water velocity. The lift-based vertical axis turbine can produce a higher coefficient of power C_P than the drag-based one, but it is still not as high of the horizontal axis turbine. This is because the blade profile is at the wrong angle of attack (AOA) during some of the the cycle of the vertical axis turbine (Korakianitis et al, 2015). This can be partly

mitgated using a variable pitch for the blades, setting the blade orietation counsility during the cycle in order to place it in a way of producing high hydrodynamic efficiency (lift to drag ratio) most of the cycle. This method has gained good interest where for example coupling this approach with computational fluid dynamics (CFD) design has been suggested (Ouayle & Rennie, 2007). However, it also leads to complexity in terms of additional machinery on the turbine and appropriate pitch-control which we try to avoid in this study.

Other methods that follow the spirit of simplicity as one would wish to find in small to medium low cost marine current turbines is passive control. This can be achieved by maintaining the vertical axis turbine at high TSR, but this may cause the turbine to miss the optimal coefficient of power C_P. One can try to delay stall on the turbines blades using a new profile design such as the presCrIbed suRface Curvature distribution bLade dEsign (CIRCLE) which seeks to remove curvature discontinuity and thus was shown to push the stall angle a few degrees by delaying the burst of the profile leading-edge septation bubble (Shen et al, 2017a,b). One can also seek to add devices of adding high lift as Gurney flaps that were found to increase the hydrodynamic efficiency of a simple H vertical turbine, i.e. turbine with straight blades, but not to delay separation (Yan et al, 2018). Micro-vortex generators (MVGs) that seek to energise the boundary layer and thus avoid its separation are also a possible engineering solution (Heffron et al, 2016). However, one should pay attention in this design that the suction and pressure surfaces of the profile switch places during the cycle and thus can affect the location and type of MVGs to be used. All these methods can be employed to try to boast the CP of the vertical axis turbine. However, they still cannot mitgate completely the problem that the profile's AOA keep changing during the rotation of the blade and thus the expected level of CP is still usually lower than that of the horizontal axis turbine that maintains a steady AOA for the blade profile for a steady incoming stream when it is properly positioned.

On the other hand, the blades of the horizontal axis marine current turbine (HAMCT) can be placed at the optimal AOA if the rotor disk is placed normal to the incoming velocity vector. For wind application this may require yaw control, but for marine currents with known and steady stream direction, the HAMCT seems to be ideally suited (Ng et al, 2013). However, the tidal current can alter its velocity direction opposite during the day, i.e. a rectilinear current. This will leave the HAMCT blades pitched at wrong angle for that direction, causing possible stall and much reduced power. This can be overcome using pitch angle control as commonly used in the wind power industry. However, the high density of the water that makes marine power so advantageous means that noticeable power can be lost by significantly pitching the blades. Thus as noted earlier due to

the additional complexity orginating from the pitch-control, such method is commonly used for very large turbines and not small to medium size.

One possible solution is the dual rotor configuration illustrated in Fig 1a. The left rotor blades are pitched at the optimal angle for flow coming from the left and the right rotor blades are optimally pitched for flow coming from the right. The rotor with the blades that is correctly-pitched to the flow is called the front rotor in this study and the other one is the rear rotor. This configuration was used for example in the legacy AK1000 turbine of Atlantis Resources Corp. However, it leaves the question what to do with the rear rotor. One way is to leave the rear rotor stationary, another option is to use rotational speed control that is common in marine turbines (Benelghali et al 2007, Singha et al 2016 and Zhu et al 2017) in order to maximise energy extraction from the rear rotor. The aim of this paper is to check whether there is potential gain in operating the rear rotor by analysing the hydrodynamic performance of a dual-rotor HAMCT.

Recently, Computational Fluid Dynamics (CFD) has been applied to solve the flow field around HAMCT, e.g. using the Large Eddy Simulation to simulate turbulent flow (Bai et al, 2014) and computing the time or phased-averaged turbulent flow using the RANS approach (Karthikeya et al, 2016). Although these methods have the potential to produce accurate results while providing insight into the physics of the flow, their computational cost can be of time-disadvantage for feasibility study of the hydrodynamic gain of a turbine configuration. Thus in this study we have used the industrial approach of Blade Element Momentum (BEM) method which can provide accurate estimate of power and thrust, with minimal computational cost. The BEM method is coupled with the Park wake model as outlined in the next section. This is followed by analysis of numerical results of a generic dual-rotor HAMCT and a general analytical estimate of the power gain from the rear rotor.

2. Methodology

The hydrodynamic performance of the dual-rotor turbine will be calculated using the Blade Element Momentum (BEM) method and Park wake model. Each rotor is dealt separately using the BEM approach, where the incoming velocity seen by the front rotor is the water free stream velocity and the incoming velocity seen by the rear rotor is provided by the wake model.

The BEM method is commonly used for kinetic turbines and it is only briefly reviewed here. For further details the reader is referred to (Korakianitis et al, 2015 and Hansen, 2008). In the steady BEM approach the rotor disk is taken as infinitesimally thin, divided to rings and the momentum theory is used to calculate the axial force and torque for each ring assuming axial and tangential

induced velocity factors *a* and *a'* due to the blade motion, see Fig 1b. Hence the axial velocity *v* and rotational speed ω at the rotor plane are;

$$v(r)=\left[1-a(r)\right],\ \ \omega(r)=\Omega\left[1+a'(r)\right]\ \ , \tag{1}$$

where r is the radial distance from the hub and Ω is the rotational speed of the rotor. The blade element theory is also used to calculate the axial force (thrust) and torque. By equating the expressions for thrust and torque by the momentum and blade element theories, one gets two non-linear equations for the two unknowns *a* & *a'*. A priori knowledge is assumed for the blade profile's lift and drag coefficients C_L & C_D variation with the angle of attack (AOA) α.

The BEM approach originates from the works of Glauert, Prandtl and Goldstein for propellers and since has gone several modifications to improve accuracy (Hansen, 2008). This includes semi-empirical expressions for hub and tip losses (Moriarty & Hansen, 2005), post-stall profile hydrodynamics (Tangler & Kocurek, 2004), stall delay due to rotational augmentation (Snel & Schepers, 1995) and for the axial force for a turbulent wake (Hansen, 2008). This axial force is commonly noted as thrust due to the propeller implication, although it points at the flow direction for the turbine and thus physicaly it is a drag force. All modifications were implemented in our BEM code that was well validated (Ai et al, 2016). The main results are the coefficients of thrust C_T and power C_P defined as;

$$C_T=\frac{T}{0.5\rho V^2 A}\ ,\ \ C_P=\frac{P}{0.5\rho V^3 A}\ \ , \tag{2}$$

where *ρ* is the water density, V is the incoming velocity and A is the area of the rotor disk. Once the axial and tangential induction factor a and a' are found per blade segement then C_T and C_P can be found by integrating the expressions given by the blade-element theory or the momentum theory along the blade span as given in the following for C_P from the momentum theory;

$$dC_P/dr=8(TSR)^2\left[1-a(r)\right]a'(r)f(r)\ \ . \tag{3}$$

TSR is the tip speed ratio, *R* is the rotor radius, *f*(r) is the blade and hub tip corrections decaying from one to zero at the vicinity of the blade's tip and hub. A similar expression can be driven for dC_T/dr by the momentum theory to be replaced by Glauret's correction for turbulent wake at $a>0.34$ (Hansen, 2008)

The effect of the rear rotor on the front one is neglected in this study. This is justified by the very fast decay of upstream propagating swirl and assuming the rear rotor is not too close to the front rotor, thus not adding a noticeable effect on its axial velocity. Such assumptions are commonly used for co-axial propulsive rotors that are much closer to each other than the current dual rotor

configuration (Leishman, 2009). The effect of the front rotor on the rear one is expressed through the Park wake model where the swirl effect is again neglected and the deficit in the axial velocity is assumed to be radially independent. Such assumptions are more accurate for the far wake of X>3−4D than for the near wake, where X is the axial distance between the two rotors and D is the rotor diameter, see Fig 1a, but the effect of downstream swirl is also commonly neglected in much closer rotors (Leishman, 2009) and as it will be seen the wake behind our front rotor is far from turbulent. Nevertheless, the downstream propagating swirl and non-radially uniform velocity deficit should be examined for low X in a future study.

Following the Park wake model the incoming velocity seen by the rear rotor is reduced by δV (Marden et al, 2013);

$$\delta V = V\left(1-\sqrt{1-C_{T,\,front}}\right)\left(\frac{D}{D+2kX}\right)^2 \quad , \tag{4}$$

where *k* is an empirical factor accounting for the spread of the wake and is taken as 0.04 (Marden et al, 2013). In the unlikely case of a turbulent wake behind the front rotor, i.e. $C_{T,front}>1$, the square root of $1-C_{T,front}$ should be replaced by 2*a*. The turbine overall coefficients are taken as;

$$C_{T,\,turbine} = C_{T,\,front} + \left(1-\delta V/V\right)^2 C_{T,\,rear} \quad , \tag{5}$$

$$C_{P,\,turbine} = C_{P,\,front} + \left(1-\delta V/V\right)^3 C_{P,\,rear} \quad , \tag{6}$$

when normalised by the free stream velocity V.

3. Numerical results and analysis of dual-rotor turbines

Commonly, single rotor HAMCTs are based on asymmetric profiles such as the E387 of Luznik et al's (2013) lab-size turbine of 46 cm diameter. However, numerical experimentation using the BEM and Park models has showed that there was little or no benefit operating a rear rotor based on such asymmetric profile. On the other hand, a noticeable benefit of increase in overall C_P was found when the blade profile was replaced by a symmetric profile as the NACA 00XX family. Thus the following results are based on the common NACA0012 and NACA0018 profiles.

The three-blade HAMCT of Luznik et al (2013) was used as the base geometric configuration where a rear rotor was added. The blades were re-pitched according to $\theta = \theta_T/(r/R)$ to achieve optimal performance in terms of C_P for high TSR, see section 4. The subscript T stands for tip condition, *r* is the radial distance from the hub and *R* is the rotor's radius. The C_P & C_T variations with TSR are plotted in Figs 2 for a single rotor tip-pitched at $\theta_T=(-2^0, 0, 2^0)$, when taking C_L and C_D variation with AOA for the NACA0012 of Re_C=135K (c is the chord length) (Shen et al, 2017). This Re_C is expected for this lab-size turbine (Ai et al, 2016 and Luznik et al, 2013). It is seen that the

rotor of $\theta_T=2^0$, produces the highest C_P almost up to 0.4, that is close to the C_P produced using the asymmetric profile E387 for this rotor (Ai et al, 2016). On the other hand, the rotor of $\theta_T=-2^0$ has the lowest C_P that becomes negative at high TSR. This is as expected, since a negative θ_T places the profile opposite to the desired pitch angle illustrated in Fig 1b. The negative pitch angle and high TSR also yields a C_T much larger than one as in Fig 2b, i.e. a turbulent wake behind the rotor. As a positive pitch angle is optimal for power performance, we expect the rear rotor will be at negative pitch angle as relative the wake velocity coming from the front rotor.

The distribution of the AOA and profile's hydrodynamic efficiency C_L/C_D along the blade's span are shown in Figs 3 for TSR=4.25 which is close to the maximum of C_P for $\theta_T=2^0$. The AOA for $\theta_T=-2^0$ is well above the stall angle of about 12^0 for most of the blade except towards the tip. As result the rotor mostly operates in a post-stall condition giving a low hydrodynamic efficiency except towards the blade's tip, hence the low C_P in Fig 2a. Increasing θ_T to zero reduces the post stall condition by pushing it more towards the hub, but a significant improvement occurs when θ_T is increased to 2^0, resulting in an almost optimal AOA just around the AOA 11^0 of C_{Lmax} for most of the blade. This gives the very favourable C_P distribution in Fig 2a and in the desired windmill state, showing C_T lower than one in Fig 2b.

The dual-rotor's C_P variations with TSR are shown in Figs 4 for $\theta_T=(0, 2^0)$ of the front rotor, where the rear rotor has a pitch angle of negative sign of that of the front. It is seen that operating both rotors at the same TSR results in an increase of up to 20% in C_P as relative to the C_P of the front rotor seen in Fig 2a. This is because the peak of C_P is at about the same TSR for both the front and rear rotors. It results in a C_P mildly higher than that of the single rotor of E387 in Fig 4b (Ai et al, 2016), while being able to deal with a current of reversing directions. On the other hand, operating the rotors at the same rotational speed e.g. RPM, results in no improvement in the C_P.

Following Figs 3 it is clear that increasing the stall AOA will enhance the performance of the dual-rotor turbine. This can be achieved using a profile design method as our CIRCLE approach (Shen et al, 2017) or by increasing the current low Reynolds number (Jacobs and Sherman, 1937). Increasing the profile Reynolds number Re_C from 135K to 1M as in the turbines of Figs 5 means the turbine becomes of low mid-size diameter about 3.5 m. The C_P and C_T variations with TSR are shown in Figs 5 for such dual-rotor turbines based on NACA0012 profile and the commonly-used thicker NACA0018, and for $\theta_T=(2^0, -2^0)$ of the front and rear rotors respectively. The C_P improves even just for the single rotor when comparing with Fig 2a, because of the increase in the AOA of C_{Lmax} from 11^0 for the NACA0012 of Re_C=135K to $(16^0, 18^0)$ for the NACA0012&0018 of Re_C=1M

respectively. Significant improvement in C_P is seen for the dual rotor, particularly for the NACA0018-based, getting C_{Pmax} to about 0.55 which is not far from the Betz limit of 0.59. The price to pay is a high thrust at high TSR as seen in Fig 5b, mostly due to the turbulence wake behind the rear rotor as was already seen from Fig 2b.

The variation of the RPM_{rear}/RPM_{front} with TSR is shown in Fig 6. This ratio is simply $1-\delta V/V$ as expressed in Eq (4) and it is seen that the RPM of the rear rotor has to be lower than that of the front one. There is a minimum in RPM_{rear}/RPM_{front}, which is slightly after the TSR of C_{Pmax}. Increasing X reduces δV and thus increases the RPM ratio as seen in Fig 6.

4. Analytical estimate of the additional power from the rear rotor

The previous section showed gains of 10% to 20% in power by operating the rear rotor. To show this is of no coincidence of that particular turbine, an analytic estimate is given assuming the front rotor is optimally pitched while the rear rotor works entirely in post-stall conditions. Following Fig 1b one can write;

$$\tan\phi=\frac{V(1-a)}{\omega r(1+a')}=\frac{(1-a)}{TSR(1+a')x} \quad , \tag{7}$$

where $x \equiv r/R$. At high TSR >> 1, we can assume that ϕ << 1 rad and a' << 1 (Korakianitis et al, 2015 and Karthikeya et al, 2016), thus

$$\phi=\frac{1-a}{TSR\ x}=\frac{\phi_T}{x} \quad , \tag{8}$$

where the subscript T denotes blade tip condition. Linear aerodynamics is assumed, i.e. $C_L=C_{L\alpha}\alpha$ and the profile drag coefficient C_{D0} is assumed to be independent of AOA. Then the maximum C_P by the BEM model and when neglecting tip edge effects is;

$$C_{P,opt}=0.5(TSR)^3\sigma\phi_T C_{L\alpha}(\phi_T-\theta_T)-0.25\sigma C_{D0}(TSR)^3 \quad , \tag{9}$$

where σ is the solidity of the rotor; $\sigma = (b\ c_{gr})/(\pi R)$. b is the number of the blades and c_{gr} is the blade mean geometric chord length. In deriving Eq (9) it was assumed there is no or little variation in the $C_{L\alpha}$ and C_{D0} along the blade's span.

One can also show that for an optimal blade, its geometric twist follows $\theta = \theta_T/x$, where by the BEM model (Korakianitis et al, 2015);

$$\theta_T=\frac{2}{3\ TSR_{opt}}\left(1-\frac{8}{3\ TSR_{opt}\ C_{L\alpha}\sigma}\right) \quad , \tag{10}$$

and

$$\phi_T=\frac{2}{3\ TSR_{opt}} \quad . \tag{11}$$

Substituting Eqs (10) & (11) into Eq (9) and taking C_{D0} =0 will yield the Betz limit $C_{P,opt}$=16/27. We shall assume that the front rotor has been optimized and performs as is predicted by Eq (9). Taking C_{D0}=0.02, σ=0.1 and TSR=4, yields -0.032 for the second (viscous) term on the RHS of Eq (9) and thus that term will be neglected.

On the other hand, the rear rotor blade is placed at the wrong pitch angle towards the flow and it is assumed the all blade has stalled. A simplistic stall model is used for the profile hydrodynamics; $C_L=C_{Lmax}$ and $C_D=C_{Dmax}$ for $|\alpha|>\alpha_{stall}$. This yields after some manipulations and assuming TSR>>1 (Rosen, 1987);

$$C_{P,stall}=\frac{(TSR)^2\sigma C_{L\,max}}{6}-\frac{8}{(TSR)^4\sigma^2 C_{L\,max}^2}\,f(W)-\frac{\sigma C_{D\,max}(TSR)^3}{4}\quad , \tag{12}$$

where

$$f(W)=\frac{W^7}{7}-\frac{2W^5}{5}+\frac{W^3}{3}-\frac{8}{105}\ ,\ W\equiv\sqrt{1-0.5\sigma C_{L\,max}(TSR)^2}\quad . \tag{13}$$

Obviously this model holds as long as W is a real number. Taking typical values of C_{Lmax}= 1, C_{Dmax}=0.1, σ=0.1, TSR=4, yields the values of 0.27, 0.17 and -0.16 for the 1st, 2nd and 3rd terms on the RHS of Eq (12) respectively. Thus only the 1st term will be accounted.

The C_P of the rear rotor will be taken as of Eq (12), but it is to be normalised according to Eq (6). Neglecting viscous effect for the front rotor yields $C_T\approx 8/9$ and assuming $C_{L\alpha}(\phi_T-\theta_T)=C_{Lmax}$ for the front rotor leads to;

$$\frac{P_{rear\ rotor}}{P_{front\ rotor}}=(0.07,0.12)\ \ for\ \ X=(2,4)D\quad . \tag{14}$$

This is at lower end of the power gain estimates given in Section 3, where higher gains of up to 20% were recorded. This is because only part of the rear rotor operated in post-stall conditions, achieving high hydrodynamic efficiency towards the tip of the blade as in Fig 3b.

5. Conclusions

A dual-rotor HAMCT was considered for its hydrodynamic performance and power gain obtained by operating the rear rotor. Such turbine is advantageous for a rectilinear tidal current of reversing directions. It was assumed the turbine was subject to a rotational speed control but not pitch control which is common in low end cost turbines. Each rotor was optimally fixed- pitched towards its upstream incoming water velocity, making it far from optimally pitched towards the wake velocity from the other rotor. The BEM method was coupled with the Park wake model assuming no turbulent wake behind the front rotor and sufficient distance between the two rotors for the swirl to decay and wake velocity radially uniform.

A generic three-blades turbine was analysed, where it was prompted to have a symmetric blade profile; the NACA0012 and NACA0018. This is because asymmetric profile as E387 were found to be not appropriate for operating the rear rotor along with the front one. A gain of up to 20% in the overall C_P was recorded as relative to the C_P of just the front rotor, bringing the overall C_P to about 0.55 as long as the rear rotor operated at the same TSR as the front rotor. This is despite a significant part of the rear rotor towards the hub operated in post-stall conditions. A general analytical model based on the assumption of the front rotor working in optimal conditions while the rear rotor was fully in post-stall conditions gave an estimate of about 10% power gain from the rear rotor. This should be viewed as the lower range of the power gain range due to the assumption of a fully-stalled rear rotor.

The current investigation incorporated a symmetric profile as NACA0012 as comprise between the demands of the forward facing rotor and backwards facing one. As in the case of the vertical axis turbine further improvement can be sought by incorporating a symmetric profile with stall delay as of the CIRCLE-based that can particularly enhance blade hydrodynamic performance in a situation that is a comprise between the two rotors and is not optimal for each of them (Ai et al, 2018). The current analysis did not account for effects from free surface waves and close proximity between the two rotors that can enhance swirl and radial non-uniformity in the wake. These effects can be further studied. Nevertheless, this research has pointed to the good potential power gain in operating a dual-rotor HAMCT that maximises the power from the rectilinear tidal current both directions without pitch or yaw control.

Acknowledgement:

The authors thank the support of the British Council UKIERI and DST India. The 2nd author was supported by CSC China.

References

Ai K, Avital EJ, Korakianitis T, Samad A and Venkatesan N (2016) ‘Surface wave effect on marine current turbine, modelling and analysis’ *International Conference on Mechanical and Aerospace Engineering ICMAE 7th*, London pp. 180-184

Ai K, Avital EJ, Shen X, Samad A and Venkatesan N (2018) ‘The surface curvature effect on performance of a laboratory scale tidal turbine’ *IAENG World Congress on Engineering WCE-2018*, London

Bai X, Avital EJ, Munjiza A and Williams JJR (2014) ‘Numerical simulation of a marine current

turbine in free surface flow, *Renewable Energy* Vol 63, pp. 715-723

Benelghali S, Benbouzid M and Charpentier JF (2007) 'Marine tidal current electric power generation technology: State of the art & current status' ICEMDC09, Antalya, pp. 1407-1412

Charlier RH (2003) 'A sleeper awakes: tidal current power '*Renewable Sustainable Energy Review Vol* **7** No 6, pp. 515-529

Hansen MOL (2008), *Aerodynamics of Wind Turbines 2nd Ed*, Earthscan, London

Heffron A, Williams JJ and Avital EJ (2016) Flow separation and passive flow control on E387 airfoil, *54th AIAA Aerospace Sciences Meeting AIAA 2016-0324*, San Diego

Jacobs EN and Sherman A (1937) 'Airfoil section characteristics as affected by variations of the Reynolds number' *NACA-TR-586*

Karthikeya T, Ezhilsabareesh K, Samad A, Venkatesan N and Avital E (2016) 'Parametric analysis of a tidal current turbine using CFD techniques' *Renew 2016*, Lisbon, CRC Press, pp. 553-557

Korakianitis T, Rezaienia M, Shen X, Avital EJ, Munjiza A, Wen P, J Williams JJR (2015) 'Aerodynamics of wind turbine technology' *Handbook of clean energy systems*, Vol 1, pp. 1-22

Leishman JG (2009) Aerodynamic performance considerations in the design of a coaxial proprotor, *Journal of American Helicopter Society Vol* 54, 012005

Luznik L, Flack KA, Lust EE, Taylor K (2013) 'The effect of surface waves on the performance characteristics of a model tidal turbine' *Renewable Energy* Vol 58, pp. 108-114

Ng KW, Lam WH and Ng KC (2013) '2002-12: 10 years of research progress in horizontal axis marine current turbines' *Energies* Vol 6 pp. 1497-1526

Marden JR, Ruben SD and Pao LY (2013) 'A model-free approach to wind farm control using game theoretic methods' *IEEE Transaction Control System Technology* Vol 21 No 4, pp. 1207-1214

Moriarty and Hansen (2005) 'Aerodyn Theory model' *NREL/TP-500-36881*

Quayle SD and Rennie AEW (2007) 'Integrating computational fluid dynamic and prototyping technologies in the investigation of multi-element profiles of a high lift variable pitch vertical axis tidal generators' International Journal of Agile Systems Vol 2 No 2, pp 222-236

Rosen A (1987), *Wind turbines lecture notes*, Technion press, Haifa

Shen X, Avital E, Rezaienia MA, Paul G and Korakianitis T (2017) 'Computational methods for investigation of surface curvature effects on airfoil boundary layer behaviour' *Journal of Algorithms and Computational Technology* Vol 11 No 1, pp 68-82

Shen X, Avital E, Paul G, Rezaienia MA, Wen P and Korakianitis T (2017) 'Experimental study of surface curvature effects on aerodynamics of low Reynolds number airfoil for small wind turbines' *Journal of Renewable Sustaintable Energy* Vol 8 No 5, 053303

Singha O, Venkatesan N, Samad A and Avital EJ (2016) 'Modeling and controller implementation

of tidal turbine for Indian remote islands' *International Conference on Mechanical and Aerospace Engineering ICMAE 7th*, London pp. 279-284

Snel and Schepers (1995) 'Join investigation of dynamic inflow effects and implementation of an engineering method' *ECN-C--94-107*

Tangler and Kocurek (2004), 'Wind turbine post-stall airfoil performance characteristics guidelines for BEM methods', *NREL/CP-500-36900*

Yan Y, Avital EJ, Korakianitis T (2018) 'CFD analysis for the performance of Gurney flap on airfoil vertical axis turbine' *International Conference on Mechanical and Aerospace Engineering ICMAE 9th*, Budapest

Zhu W, Zhang X and Gao J (2017) 'Development of a single power controller for horizontal-axis stand alone tidal current energy system' International Journal of Global Energy Issues 10(1/2), 117-127

List of Figures:

(a) (b)

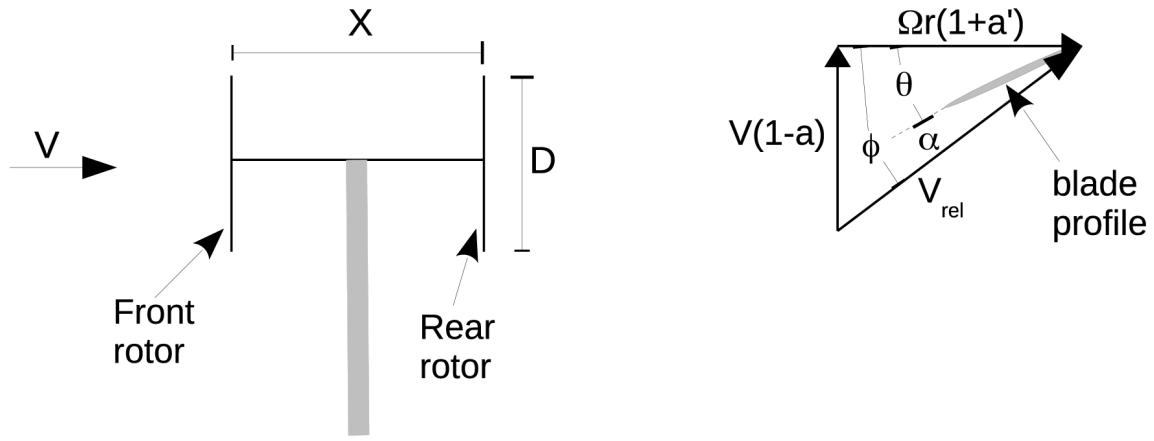

Figure 1: (a) Schematic description of the dual rotor turbine and (b) velocity vector triangle at the blade profile.

(a) (b)

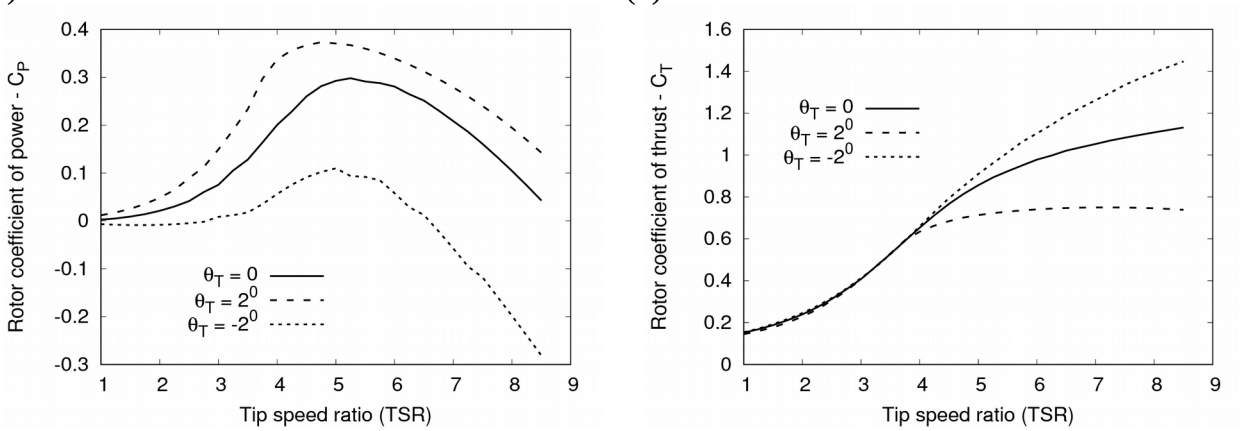

Figure 2: Rotor's coefficient of power (C_P) and thrust (C_T) variations with the tip speed ratio (TSR) of each rotor for blade profile NACA0012 and Re_C=135K

(a) (b)

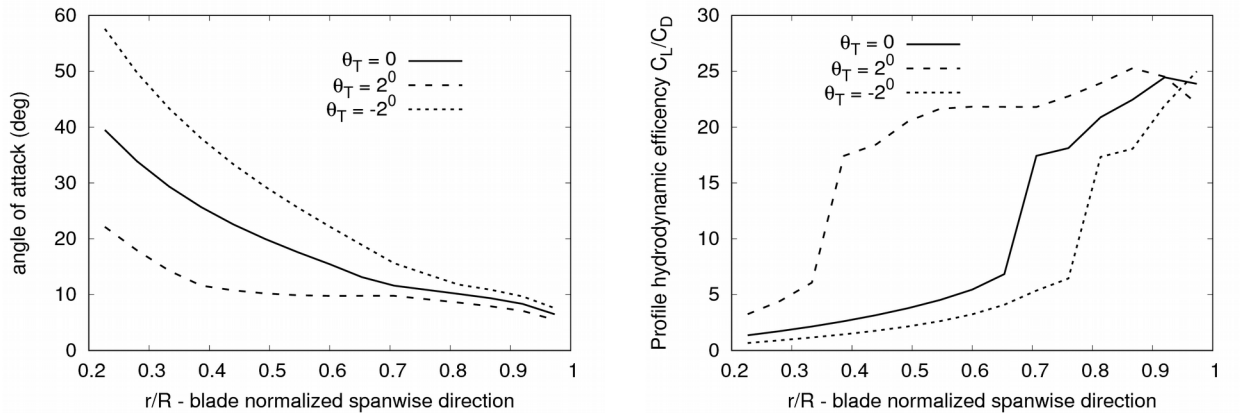

Figure 3: Angle of attack and hydrodynamic efficiency distribution along the blade for the rotors of Figs 2 and TSR=4.25

(a) (b)

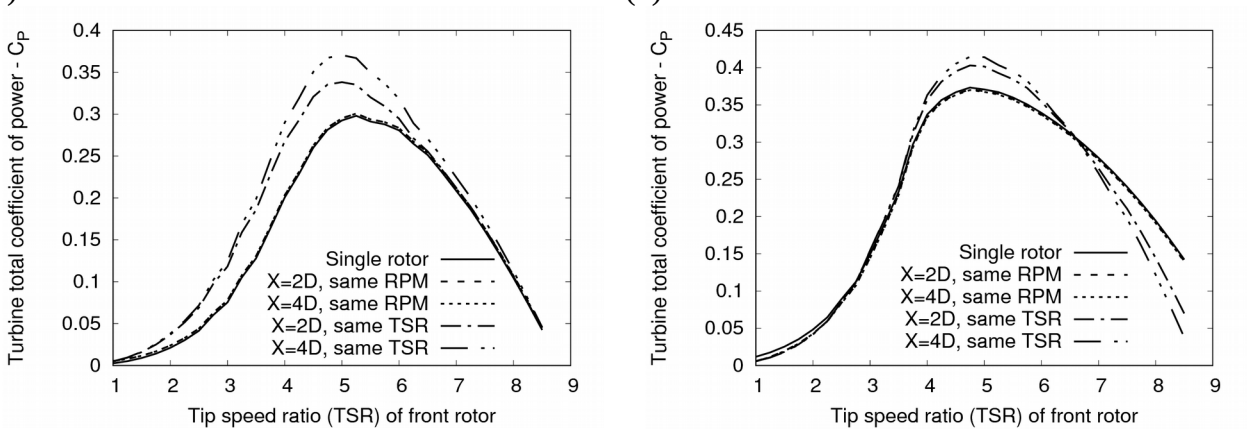

Figure 4: Turbine's total coefficient of power variation with the the front rotor TSR and tip- pitch angle (a) $\theta_T=0$ and (b) $\theta_T=2^0$. The rest of the conditions are as of Figs 2.

(a) (b)

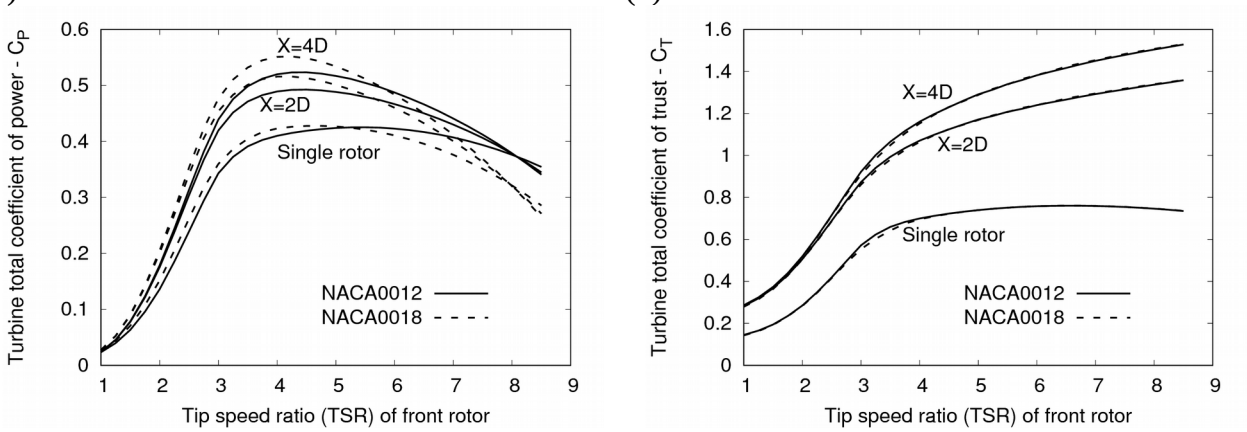

Figure 5: Turbine's total coefficient of power C_P and thrust C_T variations with the TSR of the front rotor with tip-pitch angle $\theta_T=2^0$, assuming same TSR for both rotors and Re_C=1M.

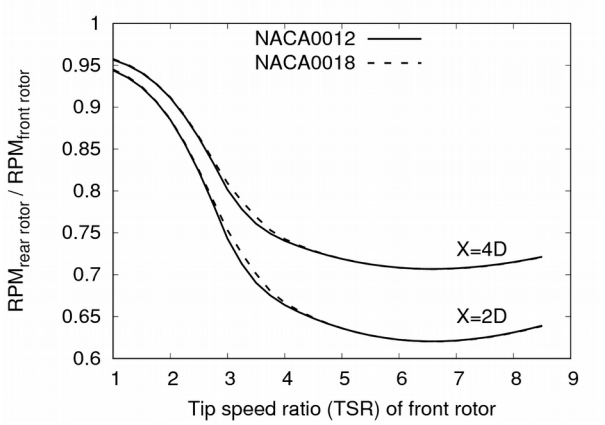

Figure 6: The variation of the RPM ratio between the two rotors of the dual-rotor turbines of Figs 5.